ADVANCING EARTH AND SPACE SCIENCES

JGR Atmospheres

RESEARCH ARTICLE
10.1029/2024JD041696

Urban Land Expansion Amplifies Surface Warming More in Dry Climate than in Wet Climate: A Global Sensitivity Study

Keer Zhang[1,2], Bowen Fang[3], Keith Oleson[4], Lei Zhao[3], Chunyang He[5,6], Qingxu Huang[5,6], Zhifeng Liu[5,6], Chang Cao[7], and Xuhui Lee[1]

[1]School of the Environment, Yale University, New Haven, CT, USA, [2]High Meadows Environmental Institute, Princeton University, Princeton, NJ, USA, [3]Department of Civil and Environmental Engineering, University of Illinois at Urbana-Champaign, Urbana, IL, USA, [4]National Center for Atmospheric Research, Boulder, CO, USA, [5]State Key Laboratory of Earth Surface Processes and Resource Ecology (ESPRE), Beijing Normal University, Beijing, China, [6]School of Natural Resources, Faculty of Geographical Science, Beijing Normal University, Beijing, China, [7]Yale-NUIST Center on Atmospheric Environment, International Joint Laboratory on Climate and Environment Change (ILCEC), Nanjing University of Information Science and Technology, Nanjing, China

Key Points:

- Climate effect of global urban land expansion is examined via a global climate model with a dynamic urban scheme
- Dry, water-limited climate regions experience a greater warming than wet, energy-limited regions
- The greater warming is caused by land-atmospheric feedback including solar brightening, soil drying, and stomatal closure

Supporting Information:

Supporting Information may be found in the online version of this article.

Correspondence to:

K. Zhang,
keer.zhang@yale.edu;
kz7693@princeton.edu

Citation:

Zhang, K., Fang, B., Oleson, K., Zhao, L., He, C., Huang, Q., et al. (2025). Urban land expansion amplifies surface warming more in dry climate than in wet climate: A global sensitivity study. *Journal of Geophysical Research: Atmospheres*, *130*, e2024JD041696. https://doi.org/10.1029/2024JD041696

Received 28 MAY 2024
Accepted 10 FEB 2025

Author Contributions:

Conceptualization: Keer Zhang, Lei Zhao, Xuhui Lee
Data curation: Keer Zhang
Formal analysis: Keer Zhang
Funding acquisition: Lei Zhao, Xuhui Lee
Investigation: Keer Zhang, Xuhui Lee
Methodology: Keer Zhang, Bowen Fang, Keith Oleson, Lei Zhao, Xuhui Lee
Project administration: Xuhui Lee
Resources: Keith Oleson, Lei Zhao, Chunyang He, Qingxu Huang, Zhifeng Liu, Chang Cao
Software: Bowen Fang, Keith Oleson
Supervision: Xuhui Lee

Abstract Urbanization changes Earth's climate by contributing to the buildup of atmospheric greenhouse gases and altering surface biophysical properties. In climate models, the greenhouse aspect is prescribed with urbanization and emission trajectories embedded in socioeconomic pathways (SSPs). However, the biophysical aspect is omitted because no models currently simulate spatially explicit urban land transition. Urban land is typically warmer than adjacent natural land due to a large urban-versus-natural land contrast in biophysical properties. The lack of biophysical representation of urbanization in climate models raises the possibility that model projection of future warming may be biased low, especially in areas with intense urban land expansion. Here, we conduct a global sensitivity study using a dynamic urban scheme in the Community Earth System Model to quantify the biophysical effect of urban land expansion under the SSP5-RCP8.5 scenario. Constant urban radiative, thermal, and morphological properties are used. We find that the biophysical effect depends on land aridity. In climate zones where surface evaporation is water-limited, the biophysical effect causes a significant increase in air temperature (0.28 ± 0.19 K; mean ± one standard deviation of nine ensemble pairs; $p < 0.01$) in areas where urban expansion exceeds 5% by 2070. The majority of this warming signal is attributed to an indirect effect associated with atmospheric and land feedback, with the direct effect of land replacement playing a minor role. These atmospheric feedback processes, including solar brightening, soil drying, and stomatal closure, act to enhance the warming initiated by surface property changes of urban land replacement.

Plain Language Summary Global urban land expansion can influence climate by changing surface properties. However, this climate effect has been omitted by all global climate models since no models can simulate urban land transition. As cities are usually warmer than rural surroundings, this omission means that future climate projections may be biased low, especially in regions with rapid urban expansion. Here, we use a global climate model with a dynamic urban scheme to investigate the climate effect of urban land expansion. We find that urban land expansion amplifies surface warming more in dry climate than in wet climate regions. This warming is mostly caused by atmospheric feedback, which enhances the small warming initiated by surface property changes. Our results underscore the need to explicitly incorporate urban land expansion in global climate models for more accurate climate projections.

1. Introduction

Urbanization, the conversion of natural landscape into built-up areas, significantly influences local climate through changing the surface biophysical properties, such as albedo, roughness, and evaporation (Hang & Chen, 2022; Lyu et al., 2024; Manoli et al., 2019; Oke et al., 2017). Current global climate models overlook the biophysical impact of global urbanization due to a lack of dynamic and spatially explicit urban land expansion in the model domain. The space-for-time substitution seems to justify this omission. First proposed for the study of deforestation climate effect (X. Lee et al., 2011; Y. Li et al., 2015), it states that the spatial difference in surface air temperature between an urban land parcel and an adjacent natural land parcel (δT_a) is equivalent to the time difference before and after the natural land parcel is urbanized (ΔT_a). Here, δT_a is the intensity of urban heat

Visualization: Keer Zhang
Writing – original draft: Keer Zhang, Xuhui Lee
Writing – review & editing: Keer Zhang, Bowen Fang, Keith Oleson, Lei Zhao, Chunyang He, Qingxu Huang, Zhifeng Liu, Chang Cao, Xuhui Lee

island. This equivalence holds if the entire natural land is replaced by urban land. More generally, the space-for-time substitution is expressed as

$$\Delta T_a = \delta T_a \times \Delta U_f \tag{1}$$

where ΔU_f is the change in urban fraction in the region of interest before and after urban land expansion. The urban land extent is currently about 1.0 million km^2 or 0.7% of the global land surface and is projected to increase to 2.3 million km^2 or 1.7% by 2070 under the SSP5 scenario with a rapid urbanization trajectory (Jing Gao & O'Neill, 2020). The global mean urban heat island intensity is about 0.9°C (Oleson et al., 2011; K. Zhang et al., 2022). Equation 1 implies that at the global scale, the direct urbanization biophysical effect is negligibly small (0.009°C). In areas with rapid urban expansion, the signal may be larger, but not by much: For grid cells that experience 10% urban expansion, the temperature change is only about 0.09°C.

As the urban and nearby natural land parcel share similar atmospheric conditions, a hidden assumption of the space-for-time substitution is that urban expansion does not change the atmospheric condition above (L. Chen & Dirmeyer, 2020). Thus, it omits land and atmospheric feedback processes, which often amplify local biophysical signals (Anderegg et al., 2019; Bonan et al., 1992). The air and the soil in cities are generally drier than their rural counterparts (Holmer & Eliasson, 1999; D. O. Lee, 1991; Meili et al., 2022; C. Tang et al., 2011). The decline in soil moisture (θ) can increase T_a, vapor pressure deficit (VPD), and sensible heat flux (H) (Anderegg et al., 2019; Berg et al., 2016). Reduction in atmospheric humidity can trigger partial stomatal closure and reduce evapotranspiration (Jianguo Gao et al., 2015; Oren & Katul, 1999; Pasqualotto et al., 2021). These responses can further enhance drying and warming associated with urban land expansion. In natural landscapes, the annual temperature difference between an open land covered by grass and its adjacent forest is negative at high latitudes (north of about 40°N) and positive at mid- to low latitudes (30°S–30°N) (X. Lee et al., 2011; Y. Li et al., 2015; Malyshev et al., 2015; T. Tang et al., 2023). Thus, the space-for-time substitution predicts that deforestation causes a reduction in the annual mean temperature at high latitudes and an increase at mid- to low latitudes. In continental deforestation modeling experiments with land and atmospheric feedbacks, this latitudinal asymmetry of the annual temperature response is enhanced substantially by a sea-ice albedo feedback at high latitudes (Bonan et al., 1992; P. J. Lawrence et al., 2012) and is influenced by a cloud feedback at low latitudes (D. Lawrence & Vandecar, 2015; Nogherotto et al., 2013; Snyder, 2010; Wang et al., 2009). In the summer season, observations show that the daily maximum temperature of open land is greater than that of its adjacent forest (M. Zhang et al., 2014), but in a large-scale, coupled deforestation numerical experiment, the cloud feedback actually causes a widespread reduction in the daily maximum temperature (L. Chen & Dirmeyer, 2020). An open question is whether future urban land expansion, which impacts much smaller land areas than these idealized continental deforestation experiments, can trigger similar atmospheric feedback.

In this study, we investigate the climate effect of global urban land expansion using a global climate model with a new dynamic urban scheme (Fang et al., 2023). The readers should consider the simulations with urban land expansion as sensitivity experiments instead of accurate climate responses to realistic urbanization. Here, we use constant urban radiative, thermal, and morphological properties in the future, despite increasing urban land cover. In the real world, urban land expansion may be accompanied by changes in urban radiative, thermal, and morphological properties because of vertical urban growth and increase in urban greenness (Chakraborty & Qian, 2024; Chi Chen et al., 2021; Frolking et al., 2024). This study focuses on the climate impact of lateral urban expansion, which is the first-order driver of regional biophysical property changes induced by urbanization.

The direct and indirect climate effects of urban expansion are separated using a factorial experiment design (Figure S1 in Supporting Information S1). The direct effect describes the climate influence of biophysical property changes caused by land replacement and the indirect effect arises from land and atmospheric feedback. We examine the magnitudes of direct and indirect climate effects and evaluate the performance of two methods in predicting the direct climate effect. Then, the climate effects of urban land expansion are analyzed in two evapotranspiration regimes. Finally, we investigate the atmospheric feedback processes responsible for the indirect climate effect of urban land expansion. The data and methodology are described in Section 2. Section 3 analyzes the direct and indirect climate effects and their mechanisms. Finally, the discussion and conclusions are presented in Sections 4 and 5, respectively.

2. Data and Methodology

2.1. Global Climate Model

The global climate model used in this study is the Community Earth System Model (CESM) version 2.1.3 (Danabasoglu et al., 2020). The atmosphere, ocean, sea ice, and land components we used are the Community Atmosphere Model version 6, Parallel Ocean Program version 2, Community Ice CodE version 5, and Community Land Model version 5 (CLM5), respectively. In CLM, the subgrid spatial heterogeneity is characterized by up to five land units (lake, glacier, urban, crop, and natural vegetation) in a grid cell, and climate contrasts in these subgrid land units or tiles represent the spatial differences between adjacent land types in the real world (D. M. Lawrence et al., 2019). The rural land tile consists of crop and natural vegetation land units. In one grid cell, the land units receive the same atmospheric forcing, but their near-surface physical state and flux variables were computed separately with their own parameterizations. For example, the urban environment was explicitly simulated by the CLM urban model based on the urban canyon concept, which accounts for the surface energy balance, hydrology, and interactions between the urban canyon and the lower atmosphere (Oleson & Feddema, 2020). The current version of CLM can only simulate constant urban land cover. In our simulations, we used a newly developed dynamic urban scheme to update urban land cover annually by reading the prescribed surface data set generated in Section 2.2 (Fang et al., 2023). Although LM3-UCM has enabled global uniform land transition between urban and vegetation lands (D. Li et al., 2016), the dynamic urban scheme developed by Fang et al. (2023) is the first scheme to enable spatial explicit urban expansion. The reader is referred to Fang et al. (2023) for a detailed description about this dynamic urban scheme.

2.2. Surface Data With Transient Urban Land

We use the transient urban land cover under the SSP5 scenario produced by He et al. (2021). As the focus of this study is the climate signal of urban land expansion, we choose the SSP5 scenario with a higher urban expansion rate than other SSP scenarios. This urban data set provides global urban land cover at a decadal interval from 2020 to 2070 at a 1-km resolution. The projection of future urban land consists of two steps. First, linear regression models, established between historical urban population and urban land area for 100×100 km grids, are used to predict future urban land demand based on the SSP5 projections of the global urban population. Second, this demand is spatially allocated at a 1-km resolution according to the suitability factor, neighborhood effect, inheritance effect, and ecological restriction. According to this projection, the global urban land area is 0.68 million km^2 in 2020, which is similar to the projections in G. Chen et al. (2020) (0.73 million km^2) and X. Li et al. (2019) (0.76 million km^2) and is smaller than the projection in Jing Gao and O'Neill (2020) (0.95 million km^2). In the projection used here, the urban extent increases to 1.3 million km^2 in 2070 (Figure 1b). In comparison, the urban extent is 2.3, 1.3, and 2.0 million km^2 in 2070 according to Jing Gao and O'Neill (2020), G. Chen et al. (2020), and X. Li et al. (2019), respectively. The differences between these urban land projections are a result of different model designs and input data. Although the RCP8.5 scenario may exaggerate future warming (Hausfather & Peters, 2020), the urban land projection used in this study is likely a conservative estimation of future urban development. If a faster urban land expansion or a different SSP scenario is adopted, we expect to find different magnitudes of climate responses.

To conduct simulations with urban expansion, we generate a new surface data set for CLM with transient urban land. We used the Toolbox for Human-Earth System Integration and Scaling (THESIS) tool set to create data layers of the urban extent and urban properties at a 0.05° resolution at the decadal time step based on the 1-km urban land cover data (Oleson & Feddema, 2020). The decadal data were then linearly interpolated to produce the annual urban data. As we plan to run simulations from 2015 to 2070 while the urban land cover data projection starts from 2020, the urban land cover from 2015 to 2019 uses the urban data at 2020. Although most cities tend to expand, a few grid cells may experience urban shrinkage. Since our focus is the impact of urban expansion, we kept the urban fraction unchanged in a grid cell if the urban extent in that grid cell starts to shrink. There are three urban density types in CLM5: tall building district (TBD), high density (HD), and medium density (MD). From the MD, HD to TBD, the urban areas are increasingly urbanized with higher buildings, less vegetation cover, and higher population density (Jackson et al., 2010). The global cities are divided into 33 urban regions, each having its unique urban biophysical properties (Jackson et al., 2010). The new urban area in each grid cell were divided into the three categories, assuming that each grid cell has the same proportions of TBD, HD, and MD as those of the CLM default urban data provided by Jackson et al. (2010). If urban land emerges in a grid cell where there is

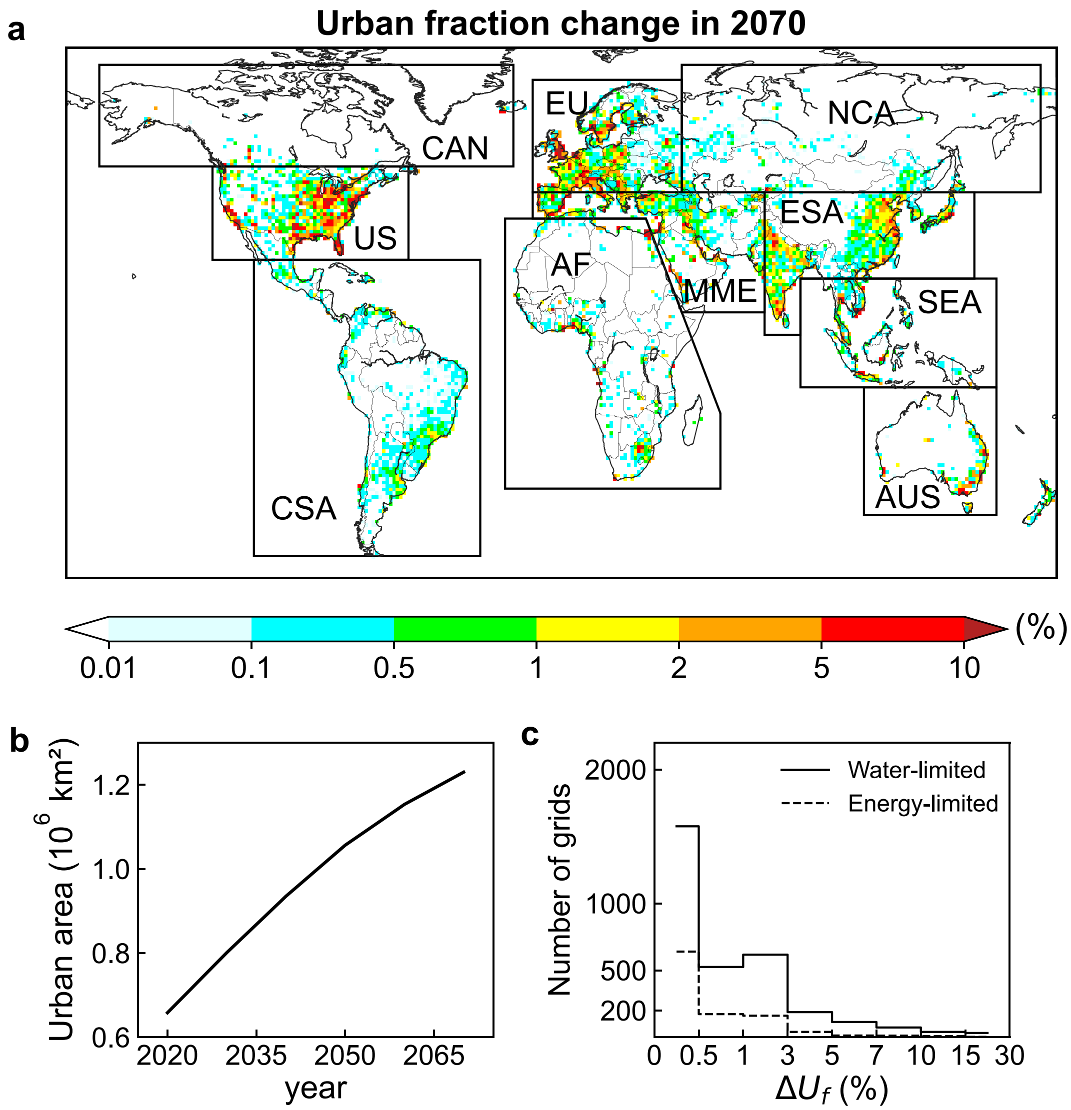

Figure 1. (a) Urban fraction change from 2020 to 2070. (b) Time series of the global urban area. (c) Histogram of urban fraction change in water-limited and energy-limited regions. The urban land cover data are from He et al. (2021). Division of 10 geographical regions denoted in panel a is created by merging AR6 reference regions (IPCC, 2021): CAN, Canada; US, United States; CSA, Central and South America; EU, Europe; AF, Africa; MME, Mediterranean and Middle East; NCA, North and Central Asia; ESA, East and South Asia; SEA, Southeast Asia; and AUS, Australia.

no urban land use in the default urban data, these proportions were assigned the average values for the urban region where the grid cell is located. Next, we used the mksurfdata_map tool to ingest the 0.05° urban data and data for other land cover types to generate a new surface data set at 0.9° × 1.25° grid resolution (Oleson & Feddema, 2020). As urban expands, other nonurban land should shrink to ensure that the five land unit fractions sum to 100% for every grid cell. We assume that urban expansion is compensated first by reduction in natural vegetation and then by cropland shrinkage in consideration of food security (Godfray et al., 2010; van Vliet, 2019; Vermeulen et al., 2012). The urban fraction change (%) in this paper refers to the changes in fraction of the urban land tile in a grid cell before and after urbanization occurs. Figure 1a shows the changes in urban fraction from 2020 to 2070.

2.3. Numerical Experiment Design

To quantify the direct and indirect climate effects of urban land expansion, we performed four sets of simulations with factorial experiment design using CESM with a 0.9° × 1.25° grid resolution (Figure S1 in Supporting Information S1).

We first conducted two sets of fully coupled simulations from 2015 to 2070 under the SSP5-RCP85 scenario, one with annual urban growth and the other with urban land use fixed at 2015. In these fully coupled simulations, all components of the CESM, including land, atmosphere, ocean, and sea ice, were active. Each simulation was repeated three times, using three different initial atmospheric and oceanic conditions in year 2015 provided by three realizations of the CESM historical simulation from CMIP6 (Danabasoglu et al., 2020; Eyring et al., 2016). The land initial condition of these fully coupled simulations was spun up by a land-only (offline) simulation with urban land use fixed at 2015. In a land-only simulation, only the land model CLM5 was active, whereas other model components used prescribed data. The spinning-up simulation was run for 40 years with atmospheric forcing cycled from 2005 to 2014, provided by a CESM historical simulation. At the end of the spinning up, the surface climate's physical state, such as air temperature and soil moisture, has reached equilibrium.

We then carried out two sets of land-only simulations from 2060 to 2070, one with annually growing urban land and another with constant urban land fixed at the 2015 level. The land initial conditions of the two simulations were provided by the land condition in year 2061 of the fully coupled simulations with constant urban land. The two simulations with and without urban expansion shared the same atmospheric forcing provided by the atmospheric output of the same fully coupled simulation providing land initial conditions. This reproduces the assumption that urban expansion does not affect atmospheric conditions in space-for-time substitution. We repeated each land-only simulation three times by using different members of fully coupled simulations with constant urban to provide the initial condition and atmospheric forcing.

The difference between the two sets of fully coupled simulations was used to represent the total biophysical effect of urban land expansion. We are interested in the surface climate of the last 10 years of simulation (2061–2070). Because by the time the model integration reached that period, the initial condition has been overwhelmed by internal climate variability, and the three dynamic urban simulations and the three constant urban simulations can be treated as being independent of each other. There are nine possible pairings of dynamic versus constant urban simulations. The total climate effect was calculated as the mean of the nine ensemble pairs. Since each fully coupled simulation is influenced by random climate internal variability, we argue that the climate differences from nine possible pairings are independent from each other, providing a higher degree of freedom in statistical tests. Our averaging period is 10 years. Many other authors have also used this length to analyze changes in the mean climate state (Chu et al., 2024; Fläschner et al., 2016; Y. Li et al., 2016; N. Zhang et al., 2010). The direct effect of urban expansion on the surface climate was calculated as the difference between the two sets of land-only simulations that shared the same atmospheric forcing. The indirect climate effect of urban expansion was calculated as the difference between the total effect and the direct effect. The fully coupled simulations are influenced by internal variability. For land-only simulations, because only the land component is active, the difference between two sets of land only simulations are not influenced by internal variability. In other words, the total and the indirect climate effects are subject to random noise. We performed *t*-tests with a sample size of nine to examine whether the total effect and indirect effect are significantly different from zero.

2.4. Evapotranspiration Regimes

Evapotranspiration plays an important role in global energy and water cycles, which drive the land-atmospheric interactions. The classical hydrology provides a simple but useful conceptual framework to divide land into two evapotranspiration regimes according to soil moisture: water-limited regime and energy-limited regime where the evaporation is controlled by soil moisture and available energy, respectively (Seneviratne et al., 2010; Vargas Zeppetelloal et al., 2019). The two regimes correspond to different degrees of land-atmospheric coupling (Hsu & Dirmeyer, 2023).

In this study, we determined the two evapotranspiration regimes with the UNEP aridity index (AI), calculated as the ratio of summer precipitation to potential evapotranspiration (UNEP, 1997). Potential evapotranspiration was estimated with the Penman equation (S. Li et al., 2016; Penman, 1948; Shuttleworth, 1993). An AI smaller than 1 indicates moisture deficit. Grid cells with AI less than 1 are defined as being water-limited, where evapotranspiration is controlled by water availability, and the rest are energy-limited where evapotranspiration is constrained by the available energy (Figures 1c and Figure S2 in Supporting Information S1). The energy-limited regions are humid, coinciding mostly with the tropical climate of the Köppen-Geiger climate classification, whereas the water-limited regions have low or intermediate wetness, largely coinciding with the temperate, dry, and boreal climates (Beck et al., 2018). The polar climate is disregarded since no urban land expansion occurs there in our urban expansion scenario.

2.5. Predicting the Direct Climate Effect of Urban Land Expansion

We used two methods to predict the direct climate effect of urban land expansion. The first approach, or space-for-time, is the application of Equation 1 using subgrid data of climate simulations and urban fraction change prescribed in the surface data (Section 1). This method is a physical process-based calculation reproducing the assumption of the direct climate effect. The results are presented in Section 3.1. The second approach, discussed in Section 4, is a "multiple linear regression method" first proposed to reconstruct the direct effect of deforestation and irrigation (Lejeune et al., 2018; Thiery et al., 2020). For each urbanizing grid cell, we applied a multiple linear regression within a 7 × 7 grid cell window as long as it contains at least 30 land grid cells and 5 urbanizing grid cells. The air temperature changes (ΔT_a) between 2015–2024 and 2061–2070 in the fully coupled simulations with urban expansion are predicted by changes in urban fraction (ΔU_f), latitude (lat), longitude (lon), and elevation (elev), such that

$$\Delta T_a = \beta_1 \times \Delta U_f + \beta_2 \times \mathrm{lat} + \beta_3 \times \mathrm{lon} + \beta_4 \times \mathrm{elev} \tag{2}$$

where ΔU_f, lat, lon, and elev are vectors containing up to 49 values, and β_i (i = 1–4) represents the regression coefficients for each predictor and is specific to each searching window. This approach is designed to statistically disentangle homogeneous climate effects with no local consequence from the heterogeneous effect due to local land replacement. The heterogeneous or direct effect of land replacement is proportional to urban fraction change, and the direct effect of the center grid cell of the moving window was calculated as β_1 times ΔU_f of this grid cell. The three spatial predictors (lat, lon, and elev) in addition to ΔU_f were used to filter out the natural climate gradient in the searching box (Lejeune et al., 2018). This method is designed to capture the direct effect of land use change and assumes other climate forcings like greenhouse gases and atmospheric feedback influence temperature identically in all grid cells in the same 7 × 7 grid cell box or searching window. An advantage of this approach is that it separates the direct and indirect climate signal of land use change with one single model simulation. We wish to determine if this economical approach can be used to study urban land expansion.

3. Results

In this Section, results are presented as the mean difference of the nine ensemble pairs for the total and the indirect climate effect and three ensemble pairs for the direct climate effect. We will use summer results (June–August in the Northern Hemisphere and December–February in the Southern Hemisphere) from 2061 to 2070, unless stated otherwise. We find that the direct effect of urban expansion is small and highly predictable, and the indirect effect dominates the temperature response to urban land expansion in areas where surface evaporation is water-limited.

3.1. Direct Versus Indirect Effect

The direct climate effect is predictable and is small in magnitude. This effect can be predicted accurately with the space-for-time substitution described by Equation 1. In the modeling system, the subgrid climate contrasts between the urban and rural land tiles within a grid cell are equivalent to the spatial difference between urban and nearby rural lands in the space-for-time substitution, denoted here with symbol δ. We used δT_a from land-only simulations and calculated ΔU_f from the surface data with transient urban land. Making use of Equation 1, we find that the predicted T_a change due to surface property changes in land replacement is in excellent agreement with the direct climate effect simulated with the land-only numerical experiments, both at the grid cell level (R^2 = 0.98, Figure 2a) and the regional level (R^2 = 0.99, Figure 2b). The direct effect of urban expansion on relative humidity (RH), sensible heat flux, and latent heat flux (λE) can also be predicted with the space-for-time substitution (Figure S3 in Supporting Information S1, $R^2 \geq 0.90$).

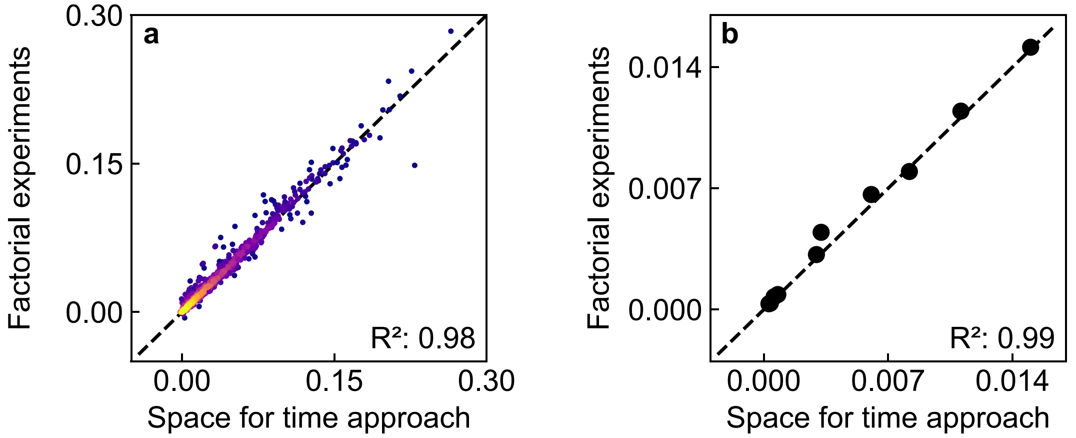

Figure 2. Comparisons between the direct effect on air temperature calculated from the space-for-time substitution method against that obtained from the factorial experiments at: (a) grid cell level, (b) regional level. The factorial experiment approach calculates the direct climate effect as the differences between land-only simulations with and without urban expansion. The space-for-time substitution approach is based on Equation 1. The dashed line is 1:1. Color in panel a indicates data density, with yellow indicating high density and purple indicating low density. The coefficient of determination (R^2) is noted. The regions in panel b are defined in Figure 1a.

Generally, the grid cell mean T_a and H increase and RH and λE decrease under the direct climate effect of urban expansion, with the magnitudes of change proportional to the urban fraction change. Of the 4216 grid cells that experience urban expansion ($\Delta U_f > 0.01\%$), 95% exhibit a T_a change less than +0.06°C. At the global scale, the T_a change is negligibly small (+0.003°C). Regionally, the mean T_a change induced by the direct effect is in the range of +0.00°C to +0.015°C, with values near the upper bound attained in regions with strong urbanization (regional $\Delta U_f > 1\%$), such as the US and Europe (Figure 3a; Figures S4a and S4b in Supporting Information S1). The standard deviations of the direct climate effect across all ensemble pairs are negligible, on the order of 0.0002°C

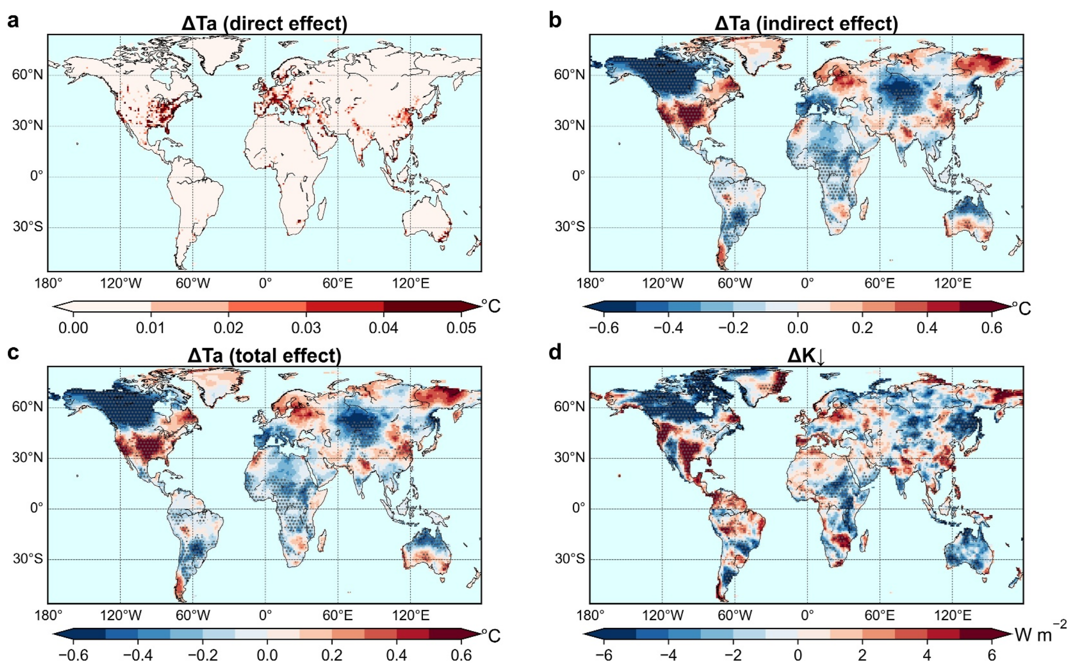

Figure 3. Spatial patterns of temperature change induced by (a) direct effect, (b) indirect effect, and (c) total effect of urbanization. (d) Spatial pattern of change in incoming solar radiation. The dotted area in panels (b–d) represents significant changes at $p < 0.05$.

or smaller, confirming that the direct effect from land-only simulations is not influenced by internal variabilities (Figure S4b in Supporting Information S1).

The indirect effect on T_a is larger in magnitude than the direct effect but is heavily influenced by internal climate variability (Figures 3a and 3b). The grid cell level T_a change induced by the indirect effect ranges from −1.6 to +1.1°C, with a greater magnitude in the mid- to high latitudes than in the tropics. However, only 29% of the 4216 grid cells that have experienced urban expansion show significance ($p < 0.05$) since the indirect effect is heavily influenced by random internal variability at the grid cell level. Regionally, the signal is significant in the US, Canada, Africa, and Central and South America ($p < 0.05$; Figure S4c in Supporting Information S1). It is difficult to draw firm conclusions for other regions because the spread is large across the model ensembles. Under the SSP5 scenario, the greatest urban expansion (1.6%) occurs in the US, so the positive indirect effect there may be linked to land use change in the same region. Land use change may also influence the climate far away by altering atmospheric circulations (Chaorong Chen et al., 2022; Devaraju et al., 2015; Laguë & Swann, 2016), a process loosely referred to as teleconnection. In Canada, the regional urban fraction change is near zero (0.03%). The large negative T_a change in Canada is likely a result of climate internal variability or a teleconnection induced by urban expansion in other regions.

3.2. Comparison Between Two Climate Regimes

We divide the land grids into energy-limited (1,051 urbanizing grid cells) and water-limited regimes (3,165 urbanizing grid cells) using an aridity threshold of unity (Section 2.4; Figures 1c and Figure S2 in Supporting Information S1). The subgrid spatial differences of surface climate variables between urban and rural lands depend on land aridity. In the water-limited regime where the climate is dry or intermediately wet, the mean δT_a, δH, and $\delta\lambda E$ under the current climate (2015–2024) are +0.99°C, +27, and −28 W m^{-2}, respectively, and are significantly larger in magnitude than their counterparts in the energy-limited regime (+0.61°C, +12, and −19 W m^{-2}; Figure 4; $p < 0.001$). These subgrid differences are highly stable over time. For instance, the mean δT_a are +0.99°C and +0.98°C in the water-limited regime in the current and the future climate (2061–2071 under the SSP5-8.5 scenario), respectively. These subgrid features have two implications. First, the subgrid climate variability under the current climate can be used to predict the direct effect of land use change in the future since the subgrid contrasts change little over time. Second, according to the space-for-time substitution (Equation 1), the larger subgrid differences in the water-limited regime mean that the direct climate effect is stronger in the water-limited climate than in the energy-limited climate for the same amount of urban expansion.

The indirect climate effect is also stronger in the water-limited regime than in the energy-limited regime. Here, we average the surface climate variables for grid cells that experience low (ΔU_f from 0.01% to 0.5%), median (ΔU_f from 0.5% to 5%), and high urban expansion ($\Delta U_f > 5\%$). The mean changes are generally insignificant for the low and median bins due to weak urban signals and large internal climate variability (Figure 5). For grid cells with high urban expansion rates in the water-limited regime, the indirect effect significantly increases T_a by 0.20°C ($p < 0.05$). This change is about twice the change attributed to the direct effect for the same grid cells. In contrast, the indirect effect on T_a is much smaller (0.04°C) and is insignificant for the high urban expansion grid cells in the energy-limited regime. For grid cells with high urban expansion, the indirect effect is to decrease RH significantly, and the RH changes are 70% (relative change) greater in the water-limited than in the energy-limited regime (Figures 5c and 5d). Intriguingly, the changes in λE and H induced by the indirect effect have opposite signs in the two climate regimes. The water-limited regions experience a decreased λE and an increased H while the reverse is true for the energy-limited regions. The opposite indirect effects on turbulent fluxes indicate that the dominant atmospheric feedback processes vary between the two climate regimes, which will be further discussed in the next section. The larger climate effects are observed in the water-limited regime in spite of higher internal climate variability than in the energy-limited regime (Figures S5a and S5b in Supporting Information S1).

The water-limited regions experience a greater total warming induced by urban expansion for areas with high urban expansion rates (0.28 ± 0.19°C; mean ± one standard deviation of nine ensemble pairs) than energy-limited regions. This local warming is about 10% of the global warming caused by GHG calculated from multi-model ensemble average projections under the SSP5-RCP8.5 scenario (Liang et al., 2020).

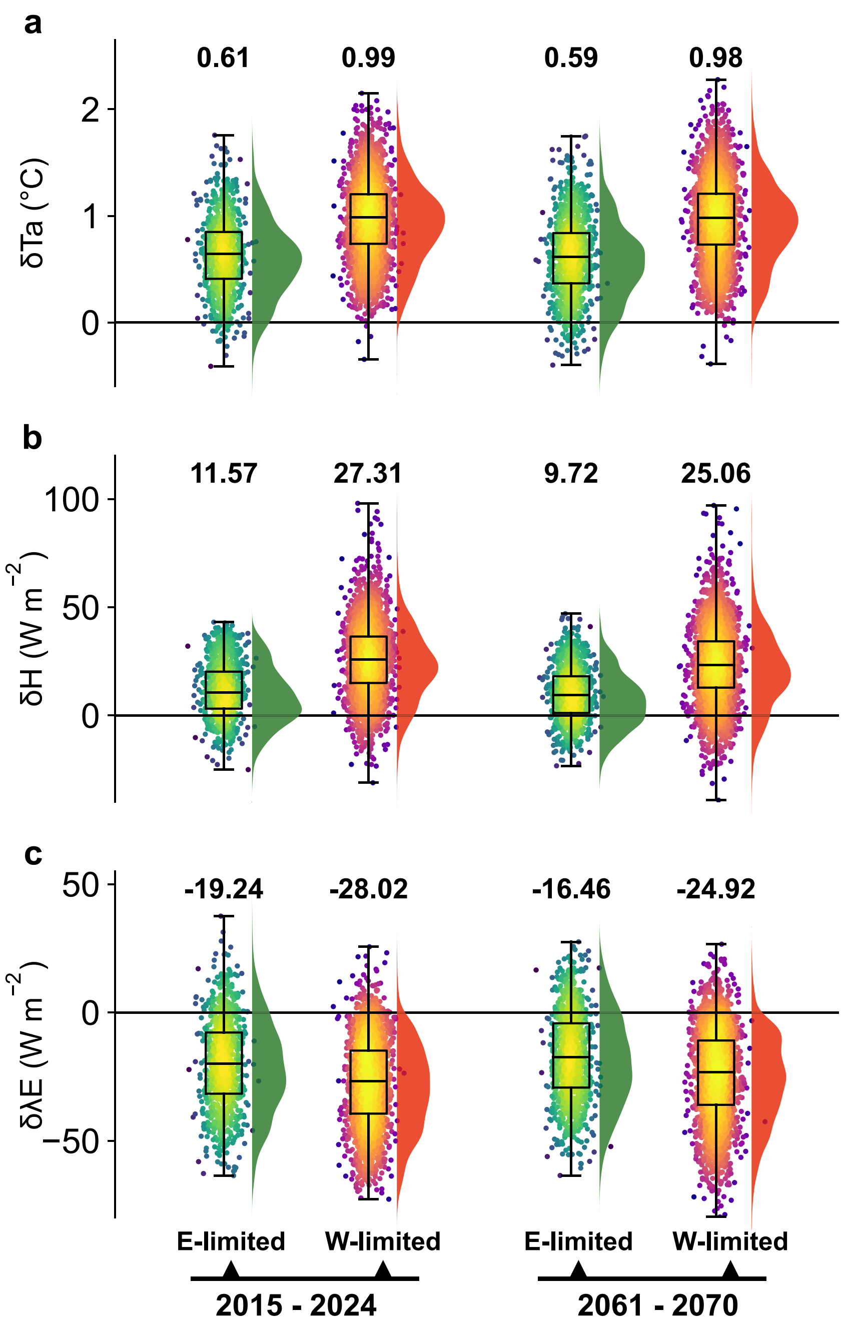

Figure 4. Subgrid spatial differences between urban and rural lands under the current and future climate: (a) Difference in air temperature, (b) difference in sensible heat flux, and (c) difference in latent heat flux. Box and whiskers show 0th, 25th, 50th, 75th, and 100th percentiles. Color indicates data density, with yellow indicating high density and green or red indicating low density. Smooth curves are probability density functions. The energy-limited (E-limited) and water-limited (W-limited) regimes mean values are denoted above the box plots.

3.3. Feedback Processes

Because humidity is generally lower in urban land than in rural land in the same model grid cell (Figure S6 in Supporting Information S1), a direct consequence of urban expansion is a reduction in the grid cell mean humidity. In areas with strong urbanization, this causes a reduction of low cloud cover and solar brightening, or an increase in the solar radiation flux incident on the surface, $K_\downarrow$ (Figure 6a and Figure S7 in Supporting Information S1). Solar brightening reinforces surface warming. This indirect effect depends on land aridity. The $K_\downarrow$

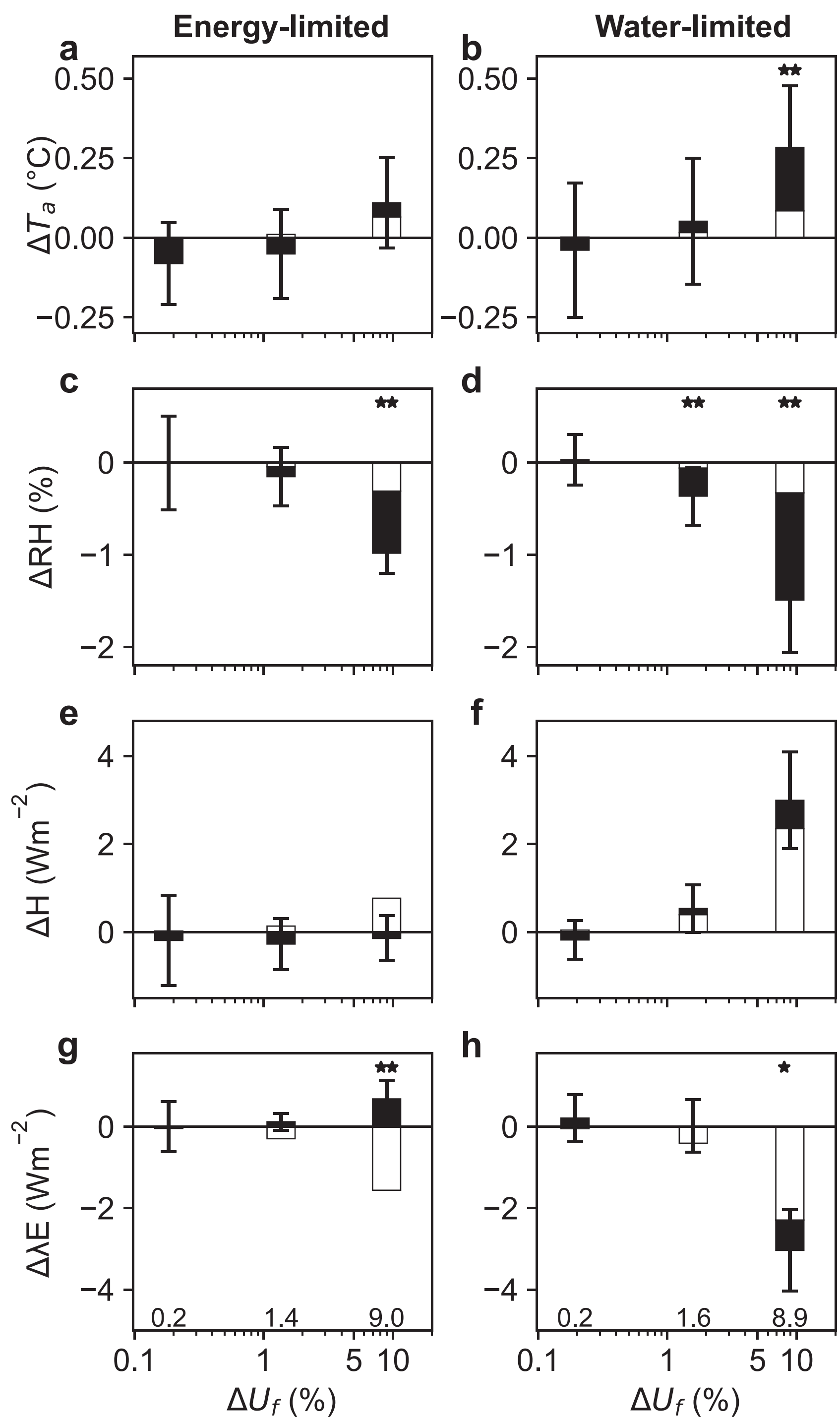

Figure 5. Comparison of changes in (a–b) air temperature, (c–d) relative humidity, (e–f) sensible heat flux, (g–h) latent heat flux between energy-limited (left column) and water-limited regions (right column). White bars: direct effect. Black bars: indirect effect. Data are presented as bin averages, with the bin average urbanization rate noted in panels (g, h). Error bars denote one standard deviation of the indirect effect across nine ensemble pairs. Significance with $p < 0.1$ and 0.05 are denoted by * and **, respectively.

change is comparable in the two regimes, increasing by 1.0 and 0.8 W m^{-2} in the water-limited and the energy-limited regimes, respectively, but the indirect effect on T_a in the water-limited regime (+0.20°C) is an order of magnitude greater than in the energy-limited regime (+0.04°C; Figures 6a, and 6b, and Figure S7 in Supporting

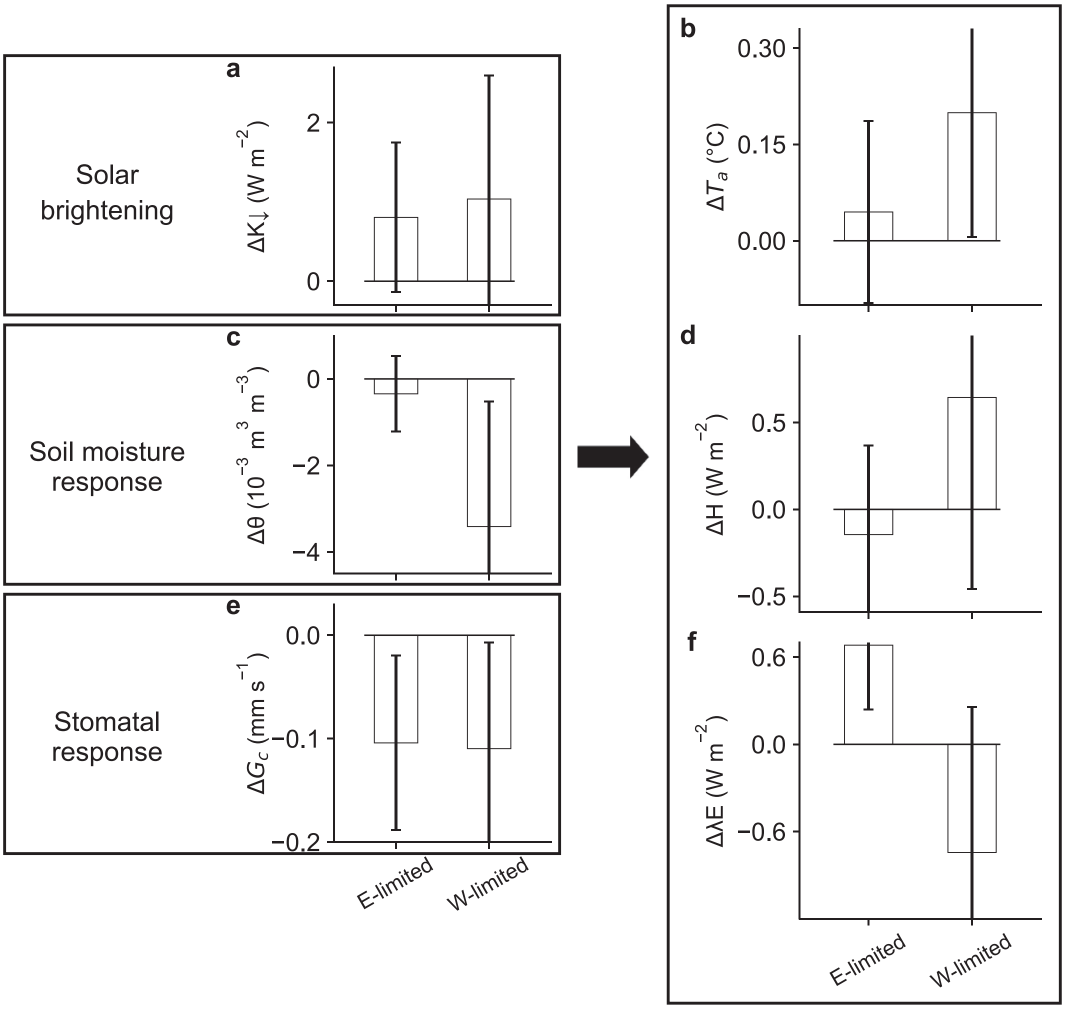

Figure 6. Comparing indirect effects for the high urban expansion grid cells in water-limited and energy-limited regions: (a) Downward solar radiation, (b) air temperature, (c) root zone (upper 92 cm) soil moisture, (d) sensible heat flux, (e) stomatal conductance, and (f) latent heat flux. Error bars denote one standard deviation of the indirect effect across nine ensemble pairs. The results are computed for grid cells that experience high urban expansion ($\Delta U_f > 5\%$).

Information S1). The low temperature sensitivity to $K_\downarrow$ in the energy-limited regime is also evident when we examine the spatial correlation between temperature and $K_\downarrow$ changes across all model grid cells (Figure S8 in Supporting Information S1). In the water-limited regime, the land surface responds to solar brightening by increasing H and reducing λE, but in the energy-limited regime where evaporation is constrained by energy availability, λE is increased and H is decreased slightly (Figures 6d, 6f and 7). The higher evaporation induced by the atmospheric feedback in the energy-limited regime acts to dampen the T_a increase and humidity decrease.

The high temperature sensitivity to solar brightening in the water-limited regime is linked to soil moisture and stomatal responses. In areas with strong urban expansion, land use change creates local drying, that is, lower RH, reduced precipitation, and lower root zone soil moisture (Figures 6c and Figure S7 in Supporting Information S1). Additionally, increased air temperature and decreased RH indicate higher VPD. Plants respond to water stress by partially closing their stomata, as indicated by the reduction in canopy conductance (G_c, Figure 6e). In the water-limited regime, stomatal closure along with lower soil moisture decreases water availability. Since evaporation is constrained by available water, soil drying and stomatal closure lead to a lower λE by 0.74 W m^{-2} or a relative decrease of 32% of the direct climate effect on λE (Figure S7 in Supporting Information S1). The reduced evaporation tends to amplify the T_a increase and the RH decrease initiated by the direct effect of urban land expansion, forming a strong positive feedback in the water-limited regime (Figure 7b). On the other hand, the changes in water availability play a minor role in humid, energy-limited regions since the evaporation is

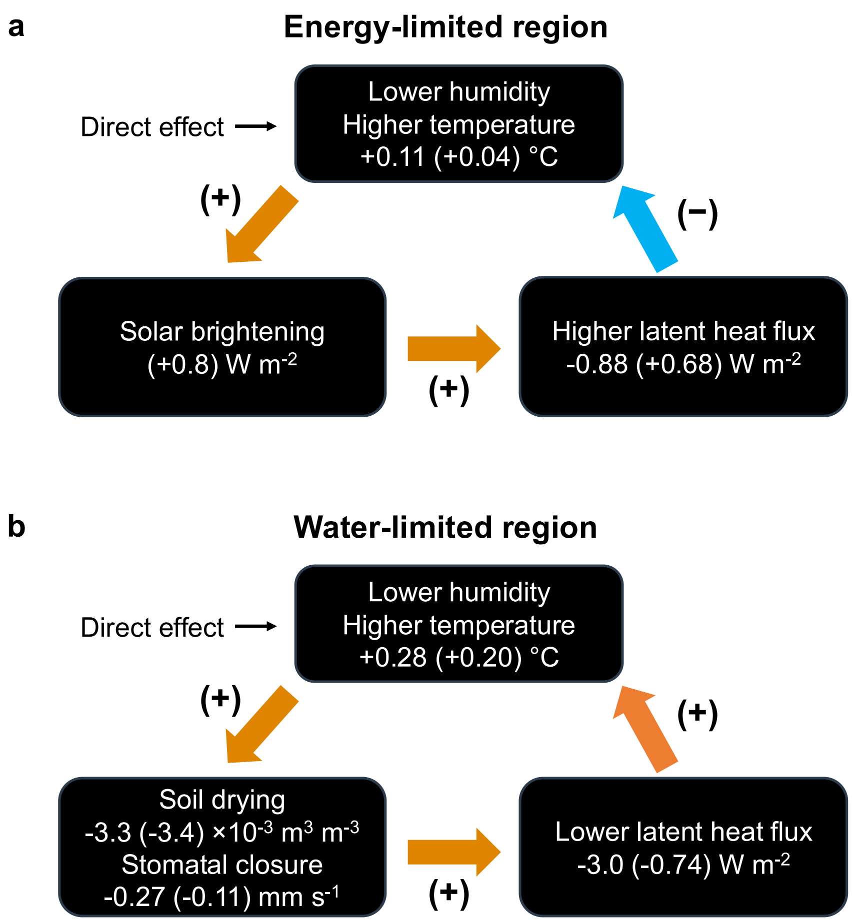

Figure 7. Land-atmospheric feedback processes in energy-limited (a) and water limited (b) regions. Orange and blue arrows indicate positive and negative effects, respectively. Values inside and outside parentheses denote indirect effects and total effects, respectively.

controlled by energy instead of water (Figure 7a). The enhanced evaporation due to atmospheric feedback dampens warming and drying initiated by land replacement.

Besides the processes in Figure 7, the sea-ice albedo feedback and water vapor feedback have been reported to enhance temperature responses to deforestation (Bonan et al., 1992; Devaraju et al., 2018; Klocke et al., 2013). Here, we examined these two processes in relation to urban land expansion, finding that their role is minor (Text S1 in Supporting Information S1).

The above discussion has focused on the period from 2061 to 2070. Analysis of the simulation results from 2051 to 2060 confirms that warming from urban land expansion is greater in the water-limited regions than in the energy-limited regions, with most of this warming signal contributed by the indirect climate effect.

4. Discussion

The feedback mechanism revealed by Figures 6 and 7 is consistent with several previous studies showing stronger atmospheric feedback to land perturbation in the water-limited regime than in the energy-limited regime (Cook et al., 2015; Devaraju et al., 2018; Seneviratne et al., 2010). For a climate system subject to natural variations, the most pronounced land-atmosphere coupling is observed in the transitional regions characterized by intermediate wetness, where evaporation variability, being constrained by soil moisture, is large enough to influence climate (Koster et al., 2006; Seneviratne et al., 2010). An inference is that, at the same strength of land perturbation, the atmospheric feedback will be stronger in dry and intermediate wetness regions than in the wet, energy-limited regions since the soil moisture-evaporation coupling increases with dryness (Seneviratne et al., 2010). This explains why the temperature reduction resulting from a unit amount of irrigation is weaker in the wet regions than in the dry and intermediate regions (Cook et al., 2015; Sacks et al., 2009). In a global deforestation numerical experiment, the indirect climate effect of deforestation is global cooling, with stronger magnitudes in mid and high latitudes than in tropical regions, despite high deforestation rates in the Amazon basin and tropical Africa (L. Chen & Dirmeyer, 2020; Devaraju et al., 2018); This latitudinal gradient again indicates that the atmospheric feedback is weaker in the energy-limited regime compared to the water-limited regime. We suggest that the stronger biophysical effect of urbanization in water-limited regions than in energy-limited regions is an intrinsic characteristic of the climate system.

We have shown that by using subgrid data, the space-for-time substitution allows a precise prediction of the direct climate effect of urban land replacement. As stated in Section 2.5, an alternative approach is to use grid mean values in a moving window to perform multiple linear regression between air temperature change, land use change, elevation, latitude, and longitude (Lejeune et al., 2018; Thiery et al., 2020). The regression term associated with land use change is then taken as the direct effect of land use change. However, the direct effect of urban land expansion estimated with this multiple linear regression approach is too large (Figure S9 in Supporting Information S1). For the high urban expansion grids, these estimates are 0.21 and 0.24°C in energy-limited and water-limited regions, respectively, whereas the true direct effects are only 0.07 and 0.09°C, respectively. The regression approach assumes that grids within the moving window are influenced by the same atmospheric conditions and that any variations result from land use change within a grid cell, or variations in elevation, latitude, or longitude. Our work suggests that atmospheric feedback is not uniform even in a small window region of 7 by 7 grids. This regression approach may perform better for simulations with a higher resolution. At a finer resolution, the 7×7 grid cell windows would occupy a smaller area and the atmospheric feedback would be more homogeneous in the searching window.

A challenge in quantifying the biophysical effect of urban land expansion is that the signal is relatively weak in comparison to internal climate variability. This study is limited to an ensemble of three members in each simulation set. This ensemble gives an accurate characterization of the internal climate variability in comparison with the ensemble of 100 members generated by the CESM2 Large Ensemble Community Project (Rodgers et al., 2021) (Figure S5 in Supporting Information S1). Both show higher variability in the water-limited regime (standard deviation of 0.26°C with three members and 0.32°C with 100 members) than in the energy-limited regime (0.16°C with three members and 0.20°C with 100 members). However, with only three ensemble members, the climate effect of urbanization cannot pass statistical tests for two thirds of urbanizing grid cells, even in some areas with fast urban expansion. For example, in Europe, the regional climate effect is 0.08°C and the standard deviation of the climate effect among nine experiment pairs is 0.48°C (Figure S4c in Supporting Information S1). At least 12 members in each set are required for a signal of this strength to pass the t-test at the 95% confidence interval. Our findings underscore the need for large ensemble simulations to detect urbanization signals.

ENSO phases are a major source of internal climate variability. Using the Troup Southern Oscillation Index with a threshold of ± 7 (Wahiduzzaman et al., 2020), we find that the six fully coupled simulations experience three to four ENSO events in 2061–2070. ENSO phases may influence the direct climate effect of urban land expansion by changing UHI and UDI intensities and the indirect effect by changing the strength of atmospheric feedback. Fitria et al. (2019) reported that the UHI in cities to the west of the Pacific Ocean increases during El Niño while those to the east increases during La Niña. ENSO cycles are known to influence rainfall distribution, cloud pattern, and soil moisture (Le & Bae, 2022; K. Xu et al., 2017). How ENSO modulates atmospheric responses to urban land expansion in energy-limited and water-limited regions remains to be explored.

Several limitations related to the global climate model should be considered when interpreting the results of this study. Although CESM has been widely used to study the impact of land use change on precipitation and monsoon (H. Chen et al., 2016; Devaraju et al., 2015; Jiang et al., 2017), the coarse resolution and uncertainty in its cloud and convection scheme remain a major challenge in property simulating land-atmospheric feedback. Additionally, atmospheric feedback is scale-dependent (L. Chen & Dirmeyer, 2020; R. Xu et al., 2022). At small scales (~1 km), mesoscale circulations and convection processes may play a role. At the climate model grid scale (~100 km), these processes are not explicitly simulated. The scale effect can be further investigated using fine resolution, convection-permitting simulations.

10.1029/2024JD041696

In CLM, urban vegetation is implicitly represented as pervious ground in street canyons, which captures the enhanced evaporation due to urban vegetation. However, more complicated processes such as root water uptake and canopy drag on air motion are not explicitly represented. The model shows a good performance in simulating the latent heat flux when comparing to observations from flux towers (Lipson et al., 2023; Oleson & Feddema, 2020). The humidity decrease due to urban expansion may be overestimated in water-limited cities with irrigation activities. Despite the potential overestimation, the urban dry island is observed for many water-limited cities (Kuttler et al., 2007; Robaa, 2013; Saffell & Ellis, 2002), in agreement with the simulated urban dry island distribution across a climate wetness gradient (K. Zhang et al., 2023). The model has also reproduced the spatial patterns of multi-year mean observed air and surface urban heat islands (K. Zhang et al., 2023; Zhao et al., 2014).

The assumption that urban expansion first replaces natural vegetation and then cropland, although reasonable, may not always hold. Cropland is generally warmer than the primary and secondary land (forest, grassland, and bare soil) in low latitudes and colder in the mid- to high latitudes (T. Tang et al., 2023). In tropical regions, if urban expansion reduces the cropland first, the direct and indirect climate effects may be weaker than those shown by our simulations, and the reverse may be true in mid- to high latitudes. This uncertainty depends on the location and cropland management regime, but it is unlikely to change our conclusions.

In our study, we have omitted future changes in urban density or in biophysical properties. Historically, cities have been growing both outward and upward (Frolking et al., 2024) and urban green coverage has been changing (Chi Chen et al., 2021; Richards & Belcher, 2019; Yang et al., 2014). If these changes continue, future urban areas may have different radiative, thermal, and morphological properties (Chakraborty & Qian, 2024). However, we consider lateral urban expansion as the first-order driver of regional biophysical property changes (Richards & Belcher, 2019). This is because urban versus rural contrast in biophysical properties is much larger than variations of these properties among built-up lands. For example, in our simulations, the urban-rural albedo contrast (mean value: 0.05) is much larger than the contrast among cities with various development levels (maximum contrast: 0.015) across the US. A national level remote sensing analysis found that the median of urban vegetation fraction decreased slightly from 47% to 42% from 2000 to 2015, especially in rapidly developing countries in Africa, Asia, and South America (Richards & Belcher, 2019). In another related study, Chakraborty and Qian (2024) found that urbanization tends to reduce regional greenness, albedo, and roughness in most areas, and this urban signal has become stronger from 2003 to 2019. If these trends continue into the future, they are more likely to enhance warming and drying caused by urban land expansion and therefore lead to stronger land-atmospheric feedback processes shown in Figure 7 and are less likely to reverse the direction of these feedback processes. We hope this study encourages more efforts to develop future projections of urban properties, including building height and vegetation fraction.

5. Conclusions

Currently, the biophysical effect of urban expansion has been overlooked in all climate projections because none of the climate models can simulate spatially explicit urban expansion. In this study, we use CESM with a new dynamic urban scheme to examine the direct and indirect climate effect of global urban land expansion. The direct climate effect due to surface property changes in urban land transition is small in magnitude and highly predictable. The space-for-time substitution equation (Equation 1) predicts the direct climate effect accurately using urban-rural climate spatial contrasts and urban fraction change. At the same amount of urban expansion, the direct climate effect is stronger in the drier water-limited climate regime than in the more humid energy-limited regime.

The indirect climate effect due to land-atmospheric feedback is larger than the direct climate effect but its grid level value is heavily influenced by internal climate variability. For grids with urban expansion exceeding 5% in 2070, the indirect effect significantly increases air temperature by 0.2°C in the water-limited regime, which is greater than the increase in the energy-limited regime (0.04°C). The stronger indirect climate effect in the water-limited regime is explained by three atmospheric feedback processes: solar brightening, regional drying, and stomatal closure. These responses lead to increased sensible heat flux and decreased latent heat flux in the water-limited regime where evaporation is limited by water availability. However, in the energy-limited regime, evaporation is not sensitive to regional drying and stomatal closure. In this regime, the increased incoming solar radiation leads to increased latent heat flux. As a result, the atmospheric feedback strongly increases air temperature in the water-limited regime, but changes temperature little in the energy-limited regime. Strong urban expansions lead to a nontrivial total warming of 0.28 and 0.11°C in the water-limited and energy-limited regions.

Our results show that it is necessary to consider global urban land expansion in the global climate model to avoid underestimating future warming, especially for dry climate regions with rapid urbanization. To accurately quantify the climate signal induced by urban land expansion, large ensemble simulations are necessary to reduce the influence of internal climate variability.

Conflict of Interest

The authors declare no conflicts of interest relevant to this study.

Data Availability Statement

The Community Earth System Model Version 2 is available at https://www.cesm.ucar.edu/models/cesm2/. The dynamic urban scheme has been released in the latest development version of the Community Terrestrial Systems Model (https://github.com/ESCOMP/CTSM). The data and Python code used to produce the figures in this paper is available on Figshare (https://doi.org/10.6084/m9.figshare.25909483.v1; K. Zhang et al., 2025).

Acknowledgments
C.C. acknowledges support by the National Natural Science Foundation of China (Grant 42021004). X.L. and L.Z. acknowledge support by the US National Science Foundation (Grants 1933630 and 2145362), L.Z. acknowledges support by the Institute for Sustainability, Energy, and Environment, and K.Z. acknowledges support by a Yale Graduate Fellowship. High-performance computing support from Cheyenne (https://doi.org/10.5065/D6RX99HX) was provided by NCAR's Computational and Information Systems Laboratory, sponsored by the US National Science Foundation.

References

Anderegg, W. R. L., Trugman, A. T., Bowling, D. R., Salvucci, G., & Tuttle, S. E. (2019). Plant functional traits and climate influence drought intensification and land – Atmosphere feedbacks. *Proceedings of the National Academy of Sciences of the United States of America* (Vol. 116(28), 14071–14076). https://doi.org/10.1073/pnas.1904747116

Beck, H. E., Zimmermann, N. E., McVicar, T. R., Vergopolan, N., Berg, A., & Wood, E. F. (2018). Present and future Köppen-Geiger climate classification maps at 1-km resolution. *Scientific Data*, *5*, 1–12. https://doi.org/10.1038/sdata.2018.214

Berg, A., Findell, K., Lintner, B., Giannini, A., Seneviratne, S. I., Hurk, B. V. D., et al. (2016). Land – Atmosphere feedbacks amplify aridity increase over land under global warming. *Nature Climate Change*, *6*(9), 869–874. https://doi.org/10.1038/NCLIMATE3029

Bonan, G. B., Pollard, D., & Thompson, S. L. (1992). Effects of boreal forest vegetation on global climate. *Nature*, *359*(6397), 1990–1992. https://doi.org/10.1038/359716a0

Chakraborty, T. C., & Qian, Y. (2024). Urbanization exacerbates continental-to regional-scale warming. *One Earth*, *7*(8), 1387–1401. https://doi.org/10.1016/j.oneear.2024.05.005

Chen, C., Ge, J., Guo, W., Cao, Y., Liu, Y., Luo, X., & Yang, L. (2022). The biophysical impacts of idealized afforestation on surface temperature in China: Local and nonlocal effects. *Journal of Climate*, *35*(23), 4233–4252. https://doi.org/10.1175/JCLI-D-22-0144.1

Chen, C., Li, D., & Keenan, T. F. (2021). Enhanced surface urban heat islands due to divergent urban-rural greening trends. *Environmental Research Letters*, *16*(12), 124071. https://doi.org/10.1088/1748-9326/ac36f8

Chen, G., Li, X., Liu, X., Chen, Y., Liang, X., Leng, J., et al. (2020). Global projections of future urban land expansion under shared socio-economic pathways. *Nature Communications*, *11*(1), 1–12. https://doi.org/10.1038/s41467-020-14386-x

Chen, H., Zhang, Y., Yu, M., Hua, W., Sun, S., Li, X., & Gao, C. (2016). Large-scale urbanization effects on Eastern Asian summer monsoon circulation and climate. *Climate Dynamics*, *47*(1–2), 117–136. https://doi.org/10.1007/s00382-015-2827-3

Chen, L., & Dirmeyer, P. A. (2020). Reconciling the disagreement between observed and simulated temperature responses to deforestation. *Nature Communications*, *11*(1), 1–10. https://doi.org/10.1038/s41467-019-14017-0

Chu, H., Cao, C., Wang, W., Xiao, W., Zhang, K., Zhang, M., & Lee, X. (2024). The land wet-bulb temperature increases faster than the sea surface temperature. *Geophysical Research Letters*, *51*(2), 1–12. https://doi.org/10.1029/2023GL106617

Cook, B. I., Shukla, S. P., Puma, M. J., & Nazarenko, L. S. (2015). Irrigation as an historical climate forcing. *Climate Dynamics*, *44*(5–6), 1715–1730. https://doi.org/10.1007/s00382-014-2204-7

Danabasoglu, G., Lamarque, J. F., Bacmeister, J., Bailey, D. A., DuVivier, A. K., Edwards, J., et al. (2020). The Community Earth System Model Version 2 (CESM2). *Journal of Advances in Modeling Earth Systems*, *12*(2), 1–35. https://doi.org/10.1029/2019MS001916

Devaraju, N., Bala, G., & Modak, A. (2015). Effects of large-scale deforestation on precipitation in the monsoon regions: Remote versus local effects. *Proceedings of the National Academy of Sciences of the United States of America* (Vol. 112(11), 3257–3262). https://doi.org/10.1073/pnas.1423439112

Devaraju, N., de Noblet-Ducoudré, N., Quesada, B., & Bala, G. (2018). Quantifying the relative importance of direct and indirect biophysical effects of deforestation on surface temperature and teleconnections. *Journal of Climate*, *31*(10), 3811–3829. https://doi.org/10.1175/JCLI-D-17-0563.1

Eyring, V., Bony, S., Meehl, G. A., Senior, C. A., Stevens, B., Stouffer, R. J., & Taylor, K. E. (2016). Overview of the Coupled Model Inter-comparison Project Phase 6 (CMIP6) experimental design and organization. *Geoscientific Model Developemnt*, *9*(5), 1937–1958. https://doi.org/10.5194/gmd-9-1937-2016

Fang, B., Zhao, L., Oleson, K., Zhang, K., Lawrence, P., Sacks, B., et al. (2023). Representing dynamic urban land change in the Community Earth System Model (CESM). *ESS Open Archive, June 14*. https://doi.org/10.22541/essoar.168676909.95382628/v1

Fitria, R., Kim, D., Baik, J., & Choi, M. (2019). Impact of biophysical mechanisms on urban heat island associated with climate variation and urban morphology. *Scientific Reports*, *9*(1), 19503. https://doi.org/10.1038/s41598-019-55847-8

Fläschner, D., Mauritsen, T., & Stevens, B. (2016). Understanding the intermodel spread in global-mean hydrological sensitivity. *Journal of Climate*, *29*(2), 801–817. https://doi.org/10.1175/JCLI-D-15-0351.1

Frolking, S., Mahtta, R., Milliman, T., Esch, T., & Seto, K. C. (2024). Global urban structural growth shows a profound shift from spreading out to building up. *Nature Cities*, *1*(9), 555–566. https://doi.org/10.1038/s44284-024-00100-1

Gao, J., & O'Neill, B. C. (2020). Mapping global urban land for the 21st century with data-driven simulations and Shared Socioeconomic Pathways. *Nature Communications*, *11*(1), 1–12. https://doi.org/10.1038/s41467-020-15788-7

Gao, J., Zhao, P., Shen, W., Niu, J., Zhu, L., & Ni, G. (2015). Biophysical limits to responses of water flux to vapor pressure deficit in seven tree species with contrasting land use regimes. *Agricultural and Forest Meteorology*, *200*, 258–269. https://doi.org/10.1016/j.agrformet.2014.10.007

Godfray, H. C. J., Beddington, J. R., Crute, I. R., Haddad, L., Lawrence, D., Muir, J. F., et al. (2010). Food security: The challenge of feeding 9 billion people. *Science*, *327*(5967), 812–818. https://doi.org/10.1126/science.1185383

Hang, J., & Chen, G. (2022). Experimental study of urban microclimate on scaled street canyons with various aspect ratios. *Urban Climate*, *46*, 101299. https://doi.org/10.1016/j.uclim.2022.101299

Hausfather, Z., & Peters, G. P. (2020). Emissions – The 'business as usual' story is misleading. *Nature*, *577*(7792), 618–620. https://doi.org/10.1038/d41586-020-00177-3

He, C., Liu, Z., Wu, J., Pan, X., Fang, Z., Li, J., & Bryan, B. A. (2021). Future global urban water scarcity and potential solutions. *Nature Communications*, *12*(1), 1–11. https://doi.org/10.1038/s41467-021-25026-3

Holmer, B., & Eliasson, I. (1999). Urban-rural vapour pressure differences and their role in the development of urban heat islands. *International Journal of Climatology*, *19*(9), 989–1009. https://doi.org/10.1002/(SICI)1097-0088(199907)19:9<989::AID-JOC410>3.0.CO;2-1

Hsu, H., & Dirmeyer, P. A. (2023). Soil moisture-evaporation coupling shifts into new gears under increasing CO_2. *Nature Communications*, *14*(1), 1162. https://doi.org/10.1038/s41467-023-36794-5

IPCC. (2021). *Climate change 2021: The physical science basis. Contribution of working group I to the sixth assessment report of the intergovernmental panel on climate change*. Cambridge University Press. https://doi.org/10.1017/9781009157896

Jackson, T. L., Feddema, J. J., Oleson, K. W., Bonan, G. B., & Bauer, J. T. (2010). Parameterization of urban characteristics for global climate modeling. *Annals of the Association of American Geographers*, *100*(4), 848–865. https://doi.org/10.1080/00045608.2010.497328

Jiang, Z., Huo, F., Ma, H., Song, J., & Dai, A. (2017). Impact of Chinese urbanization and aerosol emissions on the East Asian summer monsoon. *Journal of Climate*, *30*(3), 1019–1039. https://doi.org/10.1175/JCLI-D-15-0593.1

Klocke, D., Langen, P. L., Stevens, B., Tomassini, L., & Tomassini, L. (2013). Climate feedback efficiency and synergy. *Climate Dynamics*, *41*(9–10), 2539–2554. https://doi.org/10.1007/s00382-013-1808-7

Koster, R. D., Guo, Z., Dirmeyer, P. A., Bonan, G., Chan, E., Cox, P., et al. (2006). GLACE: The global land – Atmosphere coupling experiment. Part I: Overview. *Journal of Hydrometeorology*, *7*(4), 590–610. https://doi.org/10.1175/JHM510.1

Kuttler, W., Weber, S., Schonnefeld, J., & Hesselschwerdt, A. (2007). Urban/rural atmospheric water vapour pressure differences and urban moisture excess in Krefeld, Germany. *International Journal of Climatology*, *27*(14), 2005–2015. https://doi.org/10.1002/joc

Laguë, M. M., & Swann, A. L. S. (2016). Progressive midlatitude afforestation: Impacts on clouds, global energy transport, and precipitation. *Journal of Climate*, *29*(15), 5561–5573. https://doi.org/10.1175/jcli-d-15-0748.1

Lawrence, D., & Vandecar, K. (2015). Effects of tropical deforestation on climate and agriculture. *Nature Climate Change*, *5*(1), 27–36. https://doi.org/10.1038/nclimate2430

Lawrence, D. M., Fisher, R. A., Koven, C. D., Oleson, K. W., Swenson, S. C., Bonan, G., et al. (2019). The Community Land Model Version 5: Description of new features, benchmarking, and impact of forcing uncertainty. *Journal of Advances in Modeling Earth Systems*, *11*(12), 4245–4287. https://doi.org/10.1029/2018MS001583

Lawrence, P. J., Feddema, J. J., Bonan, G. B., Meehl, G. A., O'Neill, B. C., Oleson, K. W., et al. (2012). Simulating the biogeochemical and biogeophysical impacts of transient land cover change and wood harvest in the Community Climate System Model (CCSM4) from 1850 to 2100. *Journal of Climate*, *25*(9), 3071–3095. https://doi.org/10.1175/JCLI-D-11-00256.1

Le, T., & Bae, D. H. (2022). Causal impacts of El Niño–Southern Oscillation on global soil moisture over the period 2015–2100. *Earth's Future*, *10*(3). https://doi.org/10.1029/2021EF002522

Lee, D. O. (1991). Urban-rural humidity differences in London. *International Journal of Climatology*, *11*(5), 577–582. https://doi.org/10.1002/joc.3370110509

Lee, X., Goulden, M. L., Hollinger, D. Y., Barr, A., Black, T. A., Bohrer, G., et al. (2011). Observed increase in local cooling effect of deforestation at higher latitudes. *Nature*, *479*(7373), 384–387. https://doi.org/10.1038/nature10588

Lejeune, Q., Davin, E. L., Gudmundsson, L., Winckler, J., & Seneviratne, S. I. (2018). Historical deforestation locally increased the intensity of hot days in northern mid-latitudes. *Nature Climate Change*, *8*(5), 386–391. https://doi.org/10.1038/s41558-018-0131-z

Li, D., Malyshev, S., & Shevliakova, E. (2016). Exploring historical and future urban climate in the earth system modeling framework: 1. Model development and evaluation. *Journal of Advances in Modeling Earth Systems*, *8*, 917–935. https://doi.org/10.1002/2015MS000578

Li, S., Kang, S., Zhang, L., Zhang, J., Du, T., Tong, L., & Ding, R. (2016). Evaluation of six potential evapotranspiration models for estimating crop potential and actual evapotranspiration in arid regions. *Journal of Hydrology*, *543*, 450–461. https://doi.org/10.1016/j.jhydrol.2016.10.022

Li, X., Zhou, Y., Eom, J., Yu, S., & Asrar, G. R. (2019). Projecting global urban area growth through 2100 based on historical time series data and future shared socioeconomic pathways. *Earth's Future*, *7*(4), 351–362. https://doi.org/10.1029/2019EF001152

Li, Y., De Noblet-Ducoudré, N., Davin, E. L., Motesharrei, S., Zeng, N., Li, S., & Kalnay, E. (2016). The role of spatial scale and background climate in the latitudinal temperature response to deforestation. *Earth System Dynamics*, *7*(1), 167–181. https://doi.org/10.5194/esd-7-167-2016

Li, Y., Zhao, M., Motesharrei, S., Mu, Q., Kalnay, E., & Li, S. (2015). Local cooling and warming effects of forests based on satellite observations. *Nature Communications*, *6*(1), 6603. https://doi.org/10.1038/ncomms7603

Liang, Y., Gillett, N. P., & Monahan, A. H. M. (2020). Climate Model projections of 21st century global warming constrained using the observed warming trend geophysical Research letters. *Geophysical Research Letters*, *47*(12), 1–10. https://doi.org/10.1029/2019GL086757

Lipson, M., Grimmond, S., Best, M., Abramowitz, G., Coutts, A., Tapper, N., et al. (2023). Evaluation of 30 urban land surface models in the Urban-PLUMBER project: Phase 1 results. *Quarterly Journal of the Royal Meteorological Society*, *150*(758), 126–169. https://doi.org/10.1002/qj.4589

Lyu, H., Wang, W., Zhang, K., Cao, C., Xiao, W., & Lee, X. (2024). Factors influencing the spatial variability of air temperature urban heat island intensity in Chinese cities. *Advances in Atmospheric Sciences*, *41*(5), 817–829. https://doi.org/10.1007/s00376-023-3012-y

Malyshev, S., Shevliakova, E., Stouffer, R. J., & Pacala, S. W. (2015). Contrasting local versus regional effects of land-use-change-induced heterogeneity on historical climate: Analysis with the GFDL Earth System Model. *Journal of Climate*, *28*(13), 5448–5469. https://doi.org/10.1175/JCLI-D-14-00586.1

Manoli, G., Fatichi, S., Schläpfer, M., Yu, K., Crowther, T. W., Meili, N., et al. (2019). Magnitude of urban heat islands largely explained by climate and population. *Nature*, *573*(7772), 55–60. https://doi.org/10.1038/s41586-019-1512-9

Meili, N., Paschalis, A., Manoli, G., & Fatichi, S. (2022). Diurnal and seasonal patterns of global urban dry islands. *Environmental Research Letters*, *17*(5), 054044. https://doi.org/10.1088/1748-9326/ac68f8

Nogherotto, R., Coppola, E., Giorgi, F., & Mariotti, L. (2013). Impact of Congo basin deforestation on the African monsoon. *Atmospheric Science Letters*, *14*(1), 45–51. https://doi.org/10.1002/asl2.416

Oke, T. R., Mills, G., Christen, A., & Voogt, J. A. (2017). *Urban climates*. Cambridge University Press. https://doi.org/10.1017/9781139016476

Oleson, K. W., Bonan, G. B., Feddema, J., & Jackson, T. (2011). An examination of urban heat island characteristics in a Global Climate Model. *International Journal of Climatology*, *31*(12), 1848–1865. https://doi.org/10.1002/joc.2201

Oleson, K. W., & Feddema, J. (2020). Parameterization and surface data improvements and new capabilities for the Community Land Model Urban (CLMU). *Journal of Advances in Modeling Earth Systems*, *12*(2), 1–30. https://doi.org/10.1029/2018MS001586

Oren, R. J. S. S., & Katul, G. G. (1999). Survey and synthesis of intra- and interspecific variation in stomatal sensitivity. *Plant, Cell and Environment*, *22*, 1515–1526. https://doi.org/10.1046/j.1365-3040.1999.00513.x

Pasqualotto, G., Carraro, V., Suarez Huerta, E., & Anfodillo, T. (2021). Assessment of canopy conductance responses to vapor pressure deficit in eight hazelnut orchards across continents. *Frontiers in Plant Science*, *12*, 1–12. https://doi.org/10.3389/fpls.2021.767916

Penman, H. L. (1948). Natural evaporation from open water, bare soil and grass. *Proceedings of the Royal Society A* (Vol. 193, 120–145). https://doi.org/10.1098/rspa.1948.0037

Richards, D. R., & Belcher, R. N. (2019). Global changes in urban vegetation cover. *Remote Sensing*, *12*(1), 23. https://doi.org/10.3390/RS12010023

Robaa, S. M. (2013). Urban-suburban/rural differences over Greater Cairo, Egypt. *Atmósfera*, *16*, 157–171.

Rodgers, K. B., Lee, S. S., Rosenbloom, N., Timmermann, A., Danabasoglu, G., Deser, C., et al. (2021). Ubiquity of human-induced changes in climate variability. *Earth System Dynamics*, *12*(4), 1393–1411. https://doi.org/10.5194/esd-12-1393-2021

Sacks, W. J., Cook, B. I., Buenning, N., Levis, S., & Helkowski, J. H. (2009). Effects of global irrigation on the near-surface climate. *Climate Dynamics*, *33*, 159–175. https://doi.org/10.1007/s00382-008-0445-z

Saffell, E. M., & Ellis, A. W. (2002). Urban-rural humidity variations in Phoenix, Arizona. *Journal of the Arizona-Nevada Academy of Science*, *34*(1), 53–62.

Seneviratne, S. I., Corti, T., Davin, E. L., Hirschi, M., Jaeger, E. B., Lehner, I., et al. (2010). Investigating soil moisture-climate interactions in a changing climate: A review. *Earth-Science Reviews*, *99*(3–4), 125–161. https://doi.org/10.1016/j.earscirev.2010.02.004

Shuttleworth, W. J. (1993). Evaporation. In D. R. Maidment (Ed.), *Handbook of hydrology* (pp. 4.1–4.53). McGRAW-Hill.

Snyder, P. K. (2010). The influence of tropical deforestation on the Northern Hemisphere climate by atmospheric teleconnections. *Earth Interactions*, *14*(4), 1–34. https://doi.org/10.1175/2010EI280.1

Tang, C., Shi, B., Gao, L., Daniels, J. L., Jiang, H., & Liu, C. (2011). Urbanization effect on soil temperature in Nanjing, China. *Energy and Buildings*, *43*(11), 3090–3098. https://doi.org/10.1016/j.enbuild.2011.08.003

Tang, T., Lee, X., Schultz, N., Zhang, K., Cai, L., Lawrence, D. M., & Shevliakova, E. (2023). Biophysical impact of land use and land cover change on subgrid temperature in CMIP6 Models. *Journal of Hydrometeorology*, *24*(3), 1–37. https://doi.org/10.1175/jhm-d-22-0073.1

Thiery, W., Visser, A. J., Fischer, E. M., Hauser, M., Hirsch, A. L., Lawrence, D. M., et al. (2020). Warming of hot extremes alleviated by expanding irrigation. *Nature Communications*, *11*(290), 1–7. https://doi.org/10.1038/s41467-019-14075-4

United Nations Environment Programme. (1997). In N. Middleton & D. Thomas (Eds.), *World atlas of desertification* (2nd ed.). Retrieved from https://wedocs.unep.org/20.500.11822/30300

van Vliet, J. (2019). Direct and indirect loss of natural area from urban expansion. *Nature Sustainability*, *2*(8), 755–763. https://doi.org/10.1038/s41893-019-0340-0

Vargas Zeppetelloal, L., Battisti, D., & Baker, M. (2019). The origin of soil moisture evaporation "regimes.". *Journal of Climate*, *32*(20), 6939–6960. https://doi.org/10.1175/JCLI-D-19-0209.1

Vermeulen, S. J., Aggarwal, P. K., Ainslie, A., Angelone, C., Campbell, B. M., Challinor, A. J., et al. (2012). Options for support to agriculture and food security under climate change. *Environmental Science & Policy*, *15*(1), 136–144. https://doi.org/10.1016/j.envsci.2011.09.003

Wahiduzzaman, M., Oliver, E. C. J., Wotherspoon, S. J., & Luo, J. J. (2020). Seasonal forecasting of tropical cyclones in the North Indian Ocean region: The role of El Niño-Southern Oscillation. *Climate Dynamics*, *54*(3–4), 1571–1589. https://doi.org/10.1007/s00382-019-05075-7

Wang, J., Chagnon, F. J. F., Williams, E. R., Betts, A. K., Renno, N. O., Machado, L. A. T., et al. (2009). Impact of deforestation in the Amazon basin on cloud climatology. *Proceedings of the National Academy of Sciences of the United States of America* (Vol. 106(10), 3670–3674). https://doi.org/10.1073/pnas.0810156106

Xu, K., Tam, C. Y., Zhu, C., Liu, B., & Wang, W. (2017). CMIP5 projections of two types of El Niño and their related tropical precipitation in the Twenty-First Century. *Journal of Climate*, *30*(3), 849–864. https://doi.org/10.1175/JCLI-D-16-0413.1

Xu, R., Li, Y., Teuling, A. J., Zhao, L., Spracklen, D. V., Garcia-Carreras, L., et al. (2022). Contrasting impacts of forests on cloud cover based on satellite observations. *Nature Communications*, *13*(1), 670. https://doi.org/10.1038/s41467-022-28161-7

Yang, J., Huang, C., Zhang, Z., & Wang, L. (2014). The temporal trend of urban green coverage in major Chinese cities between 1990 and 2010. *Urban Forestry and Urban Greening*, *13*(1), 19–27. https://doi.org/10.1016/j.ufug.2013.10.002

Zhang, K., Cao, C., Chu, H., Zhao, L., Zhao, J., & Lee, X. (2023). Increased heat risk in wet climate induced by urban humid heat. *Nature*, *617*(7962), 738–742. https://doi.org/10.1038/s41586-023-05911-1

Zhang, K., Fang, B., Oleson, K., Zhao, L., He, C., Huang, Q., et al. (2025). Urban land expansion amplifies surface warming more in dry climate than in wet climate: A global sensitivity study [Dataset]. *Figshare*. https://doi.org/10.6084/m9.figshare.25909483.v1

Zhang, K., Lee, X., Schultz, N. M., Zhao, L., He, C., Huang, Q., et al. (2022). A global dataset on subgrid land surface climate (2015–2100) from the Community Earth System Model. *Geoscience Data Journal*, *10*(2), 1–12. https://doi.org/10.1002/gdj3.153

Zhang, M., Lee, X., Yu, G., Han, S., Wang, H., Yan, J., et al. (2014). Response of surface air temperature to small-scale land clearing across latitudes. *Environmental Research Letters*, *9*(3), 034002. https://doi.org/10.1088/1748-9326/9/3/034002

Zhang, N., Gao, Z., Wang, X., & Chen, Y. (2010). Modeling the impact of urbanization on the local and regional climate in Yangtze River Delta, China. *Theoretical and Applied Climatology*, *102*(3), 331–342. https://doi.org/10.1007/s00704-010-0263-1

Zhao, L., Lee, X., Smith, R. B., & Oleson, K. (2014). Strong contributions of local background climate to urban heat islands. *Nature*, *511*(7508), 216–219. https://doi.org/10.1038/nature13462